Article

Water oxidation catalyzed by cobalt oxide supported on the mattagamite phase of CoTe2.

Ian G McKendry, Akila C. Thenuwara, Jianwei Sun, Haowei Peng, John P. Perdew, Daniel R. Strongin, and Michael J. Zdilla

ACS Catal., **Just Accepted Manuscript** • DOI: 10.1021/acscatal.6b01878 • Publication Date (Web): 21 Sep 2016

Water oxidation catalyzed by cobalt oxide supported on the mattagamite phase of $CoTe_2$.

Ian G. McKendry,[‡] Akila C. Thenuwara, [‡] Jianwei Sun,[†] Haowei Peng,[†] John P. Perdew,[†] Daniel R. Strongin[‡]*, Michael J. Zdilla[‡]*

Center for the Computational Design of Functional Layered Materials, ‡Department of Chemistry, and †Department of Physics, Temple University, 1925 N. 12th St., Philadelphia, PA 19122

Supporting Information Placeholder

ABSTRACT: A chemical synthesis for the cobalt pertelluride mineral mattagamite is reported. Synthetic nanocrystalline mattagamite was investigated for electrochemical water oxidation, and showed catalytic activity. Electrochemical water oxidation occurred at an overpotential of 380 mV at 10 mA/cm^2 with a Tafel slope of 58 mV/decade and with a Faradaic efficiency of 96% and turnover frequency of 0.021 s^{-1} at 0.5V.

Keywords: Water Oxidation, Oxygen Evolution Reaction (OER), Water Splitting, Catalysis, Surface.

Introduction

Development of affordable and efficient water oxidation catalysts is the primary barrier to the realization of economically viable solar water splitting and a hydrogen economy. While nature's sole water oxidation catalyst is a pentanuclear Mn_4Ca cluster,[1] the earliest efficient synthetic water oxidation catalysts developed were heterogeneous ruthenium and iridium oxides.[2,3] Due to the high cost and low availability of Ru and Ir, the search for water oxidation catalysts has become more focused on less expensive heterogeneous materials primarily containing 1st row transition metals such as manganese,[4-9] cobalt,[10-14] nickel,[15-17] and ternary[18-20] systems such as layered double hydroxides (LDHs). Homogeneous water oxidation catalysts of first-row transition metals have made great strides in catalytic activity,[17,21-25] but are less robust than the heterogeneous systems.

Due to the high, positive electrochemical potential at which water oxidation occurs, the predominant class of heterogeneous materials being investigated comprises systems with difficult to oxidize counterions such as phosphate[13,26-28] and oxide, [2-12,14-20] with the latter group representing the bulk of the literature. This focus has presumably been due to the assumption that the heavier chalcogenides (e.g. sulfide, selenide, telluride) are more easily oxidized to their elemental phase or beyond, and would not be expected to withstand the high potentials under which water oxidation occurs. Nevertheless, increasingly frequent reports on heavy-chalgogenide-(i.e., S, Se, Te) containing water oxidation catalysts is evident. In particular, demonstration of water oxidation by synthetic $CoSe_2$[29,30] CoSe-MnO composites[31] and NiS[32] are worthy of note. Since oxidative stability decreases down a group in the periodic table, we were interested to see if water oxidation chemistry could be extended from metal sulfides and selenides to metal tellurides-supported systems. To our knowledge, a single report of a catalytic current obtained with a thin-layer coating of cobalt telluride nanotubes[33] in water solvent is the sole example of any telluride-based water oxidation catalytic system, though products of this reaction were not explicitly confirmed. Nanophases of $CoTe_2$ which catalyze the hydrogen evolution reaction have been previously reported.[34] We report here a synthesis for the orthorhombic $CoTe_2$ phase mattagamite, and demonstrate that this bulk metal-telluride phase is an excellent support for water oxidation catalysis, superior to cobalt-oxide and all heavy chalcogenides of metals so far reported.

Results and Discussion

Synthesis and Characterization

A previous report from Liang et al detailed the synthesis of layered $CoSe_2$ phases that were excellent water oxidation catalysts. We synthesized $CoSe_2$ according to the protocol of Liang et al and found that the reported synthesis and catalytic activity were reproducible in our hands. We then attempted to extend this synthetic protocol to $CoTe_2$ but were unsuccessful due to the poor solubility of Te, leading to only trace yields of unidentified products. We therefore developed a new synthesis involving the reduction of sodium tellurite (Na_2TeO_3) with hydrazine in the presence of cobalt ions. This protocol led to a good yield of a dark purple, nanocrystalline solid.

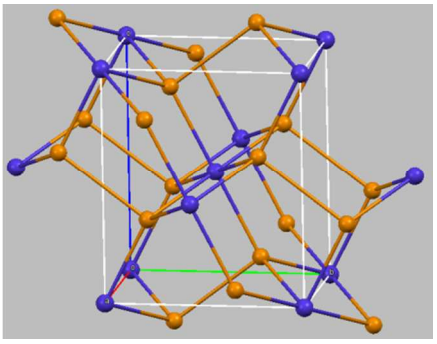

Figure 1. Structure of mattagamite ($CoTe_2$), an I-centered orthorhombic lattice of Co (blue) atoms with intervening Te_2^{2-} units (yellow).

While inductively coupled plasma optical emission spectrometry (ICP-OES) and energy dispersive spectroscopy (EDS) confirm the composition of the material as predominantly cobalt and tellurium in a ratio of 1:2 ($CoTe_2$), this material is not isomorphous with previously reported $CoSe_2$ based upon powder X-ray diffraction. A search of the American Minerologist Database revealed that this material is the known phase mattagamite, an orthorhombic cobalt pertelluride ($Co[Te_2]$, Figures 1-3).[35] The observation of a Te-Te stretch by Raman spectroscopy at ~120 cm^{-1} is similar that of elemental tellurium,[36] and supports the presence of pertelluride (Fig. S2).

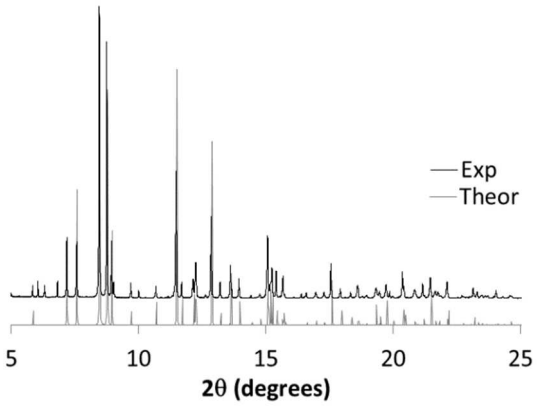

Figure 2. Powder X-ray diffraction pattern of synthetic mattagamite compared to the pattern calculated from existing crystal structure data.[35] λ = 0.414204 Å.

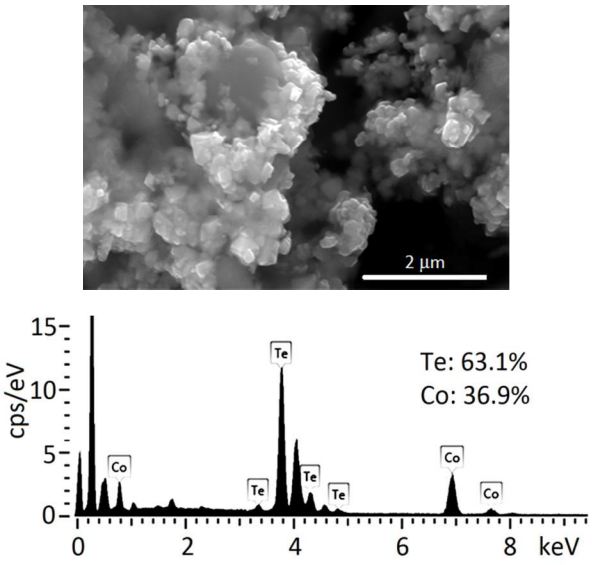

Figure 3. Scanning electron micrograph of mattagamite ($CoTe_2$) illustrating nanocrystalline structure. EDS (bottom) shows predominant Co and Te composition.

X-ray photoelectron spectroscopy (XPS) was employed to probe the surface characteristics of the synthetic mineral. The Co2*p*, Te3*d*, and O1*s* regions suggest a surface Co(II)/Te(II) oxide coating as evidenced by the presence of a Co(II) Auger shoulder feature at 785 eV in the Co 2*p* region and distinctive Te^{2+} signals at 579 and 589 eV in the Te 3*d* region, and the O1*s* peak at 533 eV is consistent with organic oxide, suggesting a surface coating of the ethanol used to rinse the crystals (Fig. S1).[37-40]

Electrochemistry and Catalysis

Electrochemical measurements on synthetic mattagamite in 1M KOH(aq) using linear sweep voltammetry reveals a catalytic current of 10 mA cm^{-2} at 380 mV above the potential for water oxidation (Figure 4), comparable to precious metal water oxidation catalysts such as iridium oxide,[3] and with a Tafel slope of ~58 mV/decade (Fig. S4). The catalytic parameters are competitive with previously reported metal-heavy-chalcogenide water oxidation catalysts.[29,31,32] (Table 1, S2). The catalyst is stable and its activity remains essentially unchanged after 1000 cycles with a gradual rise of overpotential of about 12 mV/h during chronoamperometry at 10 mA cm^{-2} (Figure 4, S10). It is worthy to note that the initial voltammogram exhibits a significant two-component oxidation wave at 1.1 and 1.2 V vs. RHE suggesting surface modification of the catalyst, which is greatly attenuated in subsequent sweeps. We attribute this to surface oxidation of both Co and Te atoms which is supported by XPS (Figure S1). Upon initial LSV sweeps, the surface Te^{2+} signal attributed to surface TeO is lost which we attribute to formation of soluble tellurate, which is expected at these high potentials, after which only pertelluride peaks remain in this region. The lost surface TeO is replaced by surface $Co^{III}O$ as evidenced by the loss of the Co $2p_{3/2}$ satellite feature indicative of Co(II) at 785 keV and growth of the Co(III) peak at 780 keV and the O1*s* peak at 530 keV consistent with formation of a surface cobalt oxide species.[40] ICP-OES on the solution supernatant over time shows a Te concentration of about 1 µL at the outset, but very little Co (0.1 µL), consistent with initial release of tellurate upon surface activation. This assignment of the active catalytic surface is consistent with the two-component oxidation pre-catalytic waves at 1.1 and 1.2 V vs. RHE in the voltammograms, which we assign to cobalt- and tellurium-based redox events that activate the catalytic surface. Thus, the active catalyst is tentatively assigned as a surface cobalt oxide layer supported by a conductive $CoTe_2$ substrate. It is likely that other heavy-chalcogenide-based water oxidation catalyst systems experience a similar surface oxide activation, though this possibility is generally not discussed.

The product of the electrolysis is confirmed using gas chromatography as O_2 (Fig. S5). Analysis of O_2 yield as a function of time over the course of 40 minutes at a current of 6 mA gives a Faradaic efficiency of 96% for this catalyst. The bulk composition of the catalyst does not change during use as determined by ICP-OES before and after catalysis, and Te and Co concentrations vary negligibly during chronoamperometry over 4 h. These results taken together suggest catalyst deactivation occurs at the surface, and not in the bulk or via leeching.

Table 1. Overpotential (η) at 10 mA cm^{-2} and Tafel slope (*b*) of CoTe compared with selected cobalt-, chalcogenide-, and bulk-phase-based OER catalysts. Expanded table available in SI, Table S2.

Compound	η (mV)	*b* (mV/dec)	pH[a]
Te-Co-O (this work)	380	58	14
$CoSe_2$ nanosheet[30]	320	44	13

$CoSe_2$ bulk[29]	380	64	14
CoTe nanotube[33]	370	--	14
Co_3O_4[41]	377	58	14
CoNi LDH[20]	367	40	14
CoOx/$CoPO_4$[42]	420	--	14
$CoFeO_x$[42]	370	--	14
$NiCoO_x$[42]	380	--	14
RuO_x[43]	390	90	15
IrO_x	380	60	14

[a] All cited samples were obtained in aqueous NaOH or KOH.

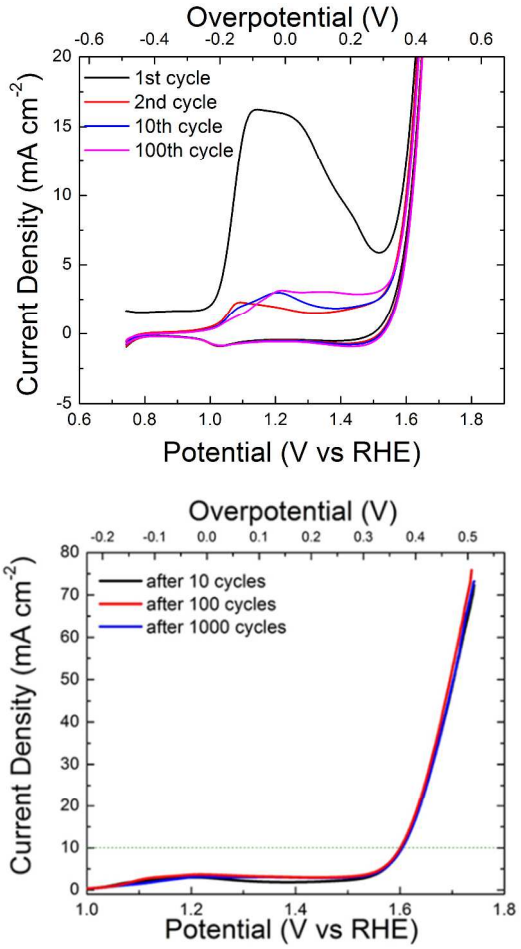

Figure 4. Cyclic (top) and Linear sweep (bottom) voltammagrams of $CoTe_2$ with η = 380 mV at 10 mA cm^{-2} and b = 42 mV/dec. Top: expanded view of early sweeps showing an initial surface activation step characterized by an oxidation wave in the range of 1.1-1.2 V vs. RHE. Upon subsequent scans this wave is greatly attenuated suggesting only traces of the associated redox species remain at the surface. Bottom: Expanded view of later scans with 10 mA cm^{-2} indicated with dotted line.

Density Functional Theoretical Calculations

For an understanding of the electronic structure basis of water oxidation by $CoTe_2$, we performed Density Functional Theoretical calculations on $CoTe_2$.[44-52] In Fig. 5, we plot the band structure and density of states for $CoTe_2$ with a low-energy anti-ferromagnetic configuration. We have sampled several anti-ferromagnetic configurations, and also the ferromagnetic configuration, all of which SCAN+rVV10[48-51] predicts to be metal-like. This finding is consistent with the UV-Visible electronic absorption spectrum of $CoTe_2$ which shows uniform absorption across the UV-Visible range (Fig. S3), indicative of a negligible band gap. Thus the populated e_g state in the CoTe support may not play a direct role in catalysis, but provides electronic conductivity that may serve to increase the rate of hole transfer to the surface catalytic cobalt oxide layer. In mattagamite CoTe2, the Co(II) ion takes the $t_2{\uparrow}^3 t_2{\downarrow}^3 e_g{\uparrow}^1 e_g{\downarrow}^0$ configuration, where t_2 and e_g denote the triply- and doubly-degenerate states due to the crystal field splitting. The DOS plot indicates delocalization of the unpaired e_g^1 orbital near the Fermi level via mixing with the pertelluride p orbitals. Such occurrence of e_g^1 states near the Fermi level has been proposed as an indicator for good oxygen evolution catalyst candidates[53,54], and has been cited in a previous study of $CoSe_2$[30].

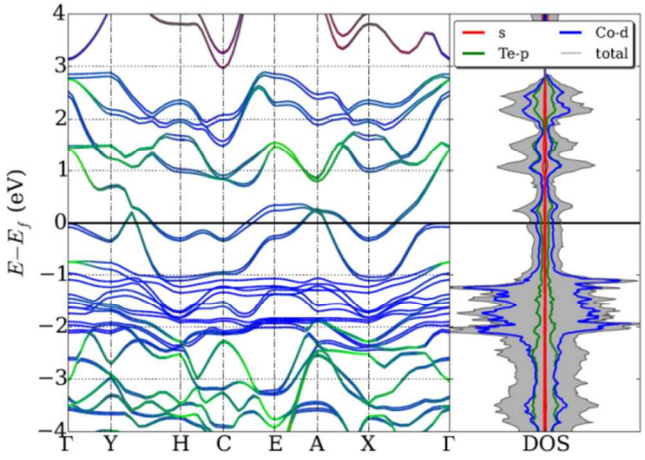

Figure 5. The calculated band structure and density of states (DOS) for CoTe2. The energy zero is set to the valence band maximum (VBM). The RGB color of the band structure represents the contribution from *s*, Te-*p*, Co-*d* states.

Conclusion

In summary, nanocrystalline mattagamite phase $CoTe_2$ is an excellent water oxidation catalyst, comparable to Co_3O_4, Co(O)OH, CoS_2, $CoSe_2$, NiS, and $CoTe_2$ nanotubes. In light of the oxidizability of telluride, it is perhaps surprising that a telluride system is able to outcompete oxides of cobalt for water oxidation activity. Preliminary results indicate that the material overcomes this challenge by the surface activation to a catalytically active species proposed to be a surface Co-O phase. Future work will experimentally and theoretically explore the mechanism of catalysis, fabrication of thin film heterostructures, and elucidation of the active crystallographic face.

Experimental

General. All reagents were purchased from commercial vendors and used without further purification. X-ray diffraction was performed on an APEX II DUO diffractometer using copper Kα1 radiation from a sealed tube, and processed using Bruker XRD² and DIFFRACEVA software packages. Linear sweep voltammetry was measured on a CHI 660E electrochemical apparatus. Faradaic efficiency was determined by time-dependent analysis of electrochemically-generated

headspace gas with a HP 5850 series II Gas Chromatograph with a molecular sieve column and a thermal conductivity detector. X-ray photoelectron spectra were obtained using a VG Scientific 100 mm hemispherical analyzer and a Physical Electronics Mg Kα X-ray source operating at 280W. Raman measurements were performed using a Horiba Labram HR800 Evo confocal Raman spectrometer with 532 nm excitation and a 100× objective. The resolution of the Raman spectrometer is about 3 cm–1. The excitation laser intensity was maintained below the sample optical damage threshold. All samples were pressed into pellets to obtain a smooth surface for Raman analysis. UV-Visible absorption spectroscopy was performed using a Shimadzu 2550 spectrophotometer with an IRS-2200 diffuse reflectance stage. Scanning electron microscopy (SEM) images were obtained using a FEI Quanta 450 FEG-SEM microscope operating at 30 kV. Energy dispersive spectroscopy (EDS) analysis was performed by an Oxford systems nanoanalysis EDS system, using Aztec 2.1 as the analyzing software. Elemental analysis was performed using a Thermo Scientific iCAP 7000 Series inductively coupled plasma optical emission spectrometer (ICP-OES). Transmission Electron Microscopy images were collected using a JEOL JEM-1400 microscope operating at 120 kV. SEM samples were prepared by depositing sample on carbon conductive tape mounted on aluminum stubs. Images were acquired on an Agilent 8500 FE-SEM operating at 1 kV.

Electrochemical Characterization

The electrochemical studies were carried out in 1 M KOH using a CHI 660E potentiostat operating in a standard three-electrode configuration at ambient temperature (22 ± 2 °C). Mirror polished glassy carbon electrode (3 mm diameter) was used as the working electrode. All the potentials were measured with respect to a standard calomel reference electrode (CH instruments) and Pt wire was used as the counter electrode. The catalyst containing ink solution was prepared by adding 4 mg of catalyst and 4 mg of carbon (VulcanXC-72), which was dispersed in 1 mL isopropanol and 35 µL of Nafion solution (5% in alcohol, Ion Power Inc.) was added as the binding agent. The resulting mixture was sonicated for at least 1 hour to form a catalyst ink. The working electrode was prepared by drop casting 5 µL of catalyst ink suspension on a 3 mm diameter glassy carbon electrode (loading 0.28 mg/cm^2). All the polarization curves were recorded at 10 mV/s scan rate. For all the catalysts tested here, polarization curves were replicated at least 5 times. The overpotential (at a current density of 10 mA/cm^2) and Tafel slopes reported are based on an analysis of these data.

Synthesis of Mattagamite. In a thick-walled pressure flask, Na_2TeO_3 (1.044g, 4 mmol) was dissolved in 10 mL distilled, deionized H_2O to which, 1 mL hydrazine hydrate (8 mmol) was added to reduce the Te^{2+} to Te^{2-}. $CoSO_4$ (0.687g, 2 mmol) dissolved in 5 mL H_2O was added to the telluride solution resulting in a lilac purple solution, which was allowed to seed for 5 minutes. After this stirring period, diethyltriamine:water (90:60 vol/vol) was added to the cobalt-tellurium solution on ice (0°C) followed by 0.837 g sodium oleate solid. The flask was then sealed and heated at 180 °C for 30 h. The resulting black precipitate was filtered and washed with ethanol. The dried powder was then annealed under air free conditions (vacuum or argon atmosphere) at 350°C for 0.5h to give sheet like mattagamite. Annealing for longer times (4 h) or at higher temperatures (425 °C) gave larger mattagamite blocks with structure and reactivity maintained.

Density Functional Theoretical Calculations

For an understanding of the electronic structure basis of water oxidation by $CoTe_2$, we performed Density Functional Theoretical calculations on $CoTe_2$. The density functional theory calculations in this study were performed with the projector augmented wave (PAW) method[44] as implemented in the VASP code.[45-47] We use the recently developed SCAN+rVV10 density functional[48] to approximate the exchange-correlation, which is built on the Strongly Constrained and Appropriately Normed (SCAN) meta-Generalized-Gradient-Approximation[49] and the revised Vydrov-van Voorhis (rVV10) non-local van der Waals correlation functional.[50,51] The ion-electron interaction was described with the PAW Perdew-Burke-Ernzerhof (PBE)[52] pseudopotentials. A plane wave basis with the cutoff energy about 400 eV, and a 10 x 8 x 6 Monkhorst-Pack k-mesh[55] 24 x 24 x 1 were used.

ASSOCIATED CONTENT

Supporting Information

Experimental procedures, X-Ray photoelectron, Raman, and electronic absorption spectra, Tafel plots, determination of faradaic efficiency, ICP-OES, TEM, and an expanded table of parameters from previously reported catalysts.[15, 16, 20, 29, 33, 42, 43, 56] This material is available free of charge via the Internet at http://pubs.acs.org."

AUTHOR INFORMATION

Corresponding Author

Michael J. Zdilla – mzdilla@temple.edu,
Daniel R. Strongin – dstrongi@temple.edu

Present Addresses

‡Department of Chemistry, Temple University, 1901 N. 13th St., Philadelphia, PA 10122

†Department of Physics, Temple University, 1925 N. 12th St., Philadelphia, PA 19122

Notes

The authors declare no competing financial interests.

ACKNOWLEDGMENT

This work was supported as part of the Center for the Computational Design of Functional Layered Materials, an Energy Frontier Research Center funded by the U.S. Department of Energy, Office of Science, Basic Energy Sciences under Award #DE-SC0012575. Use of the Advanced Photon Source at Argonne National Laboratory was supported by the U. S. Department of Energy, Office of Science, Office of Basic Energy Sciences, under Contract No. DE-AC02-06CH11357. This research used resources of the National Energy Research Scientific Computing Center (NERSC), a DOE Office of Science User Facility supported by the Office of Science of the U.S. Department of Energy. Yaroslav V. Aulin and Eric Borguet are gratefully acknowledged for assistance with Raman spectroscopy.

REFERENCES

(1) Dau, H.; Zaharieva, I.; Haumann, M. *Curr. Opin. Chem. Biol.* **2012**, *16*, 3-10.

(2) Harriman, A.; Thomas, J. M.; Millward, G. R. *New J. Chem.* **1987**, *11*, 757-762.

(3) Harriman, A.; Richoux, M.-C.; Christensen, P. A.; Mosseri, S.; Neta, P. *J. Chem. Soc. Farad. T. 1* **1987**, *83*, 3001-3014.

(4) Pokhrel, R.; Goetz, M. K.; Shaner, S. E.; Wu, X.; Stahl, S. S. *J. Am Chem. Soc.* **2015**, *137*, 8384-8387.

(5) Birkner, N.; Nayeri, S.; Pashaei, B.; Najafpour, M. M.; Casey, W. H.; Navrotsky, A. *Proc. Natl. Acad. Sci. USA* **2013**, *110*, 8801-8806.

(6) Huynh, M.; Shi, C.; Billinge, S. J. L.; Nocera, D. G. *J. Am Chem. Soc.* **2015**, *137*, 14887-14904.

(7) Indra, A.; Menezes, P. W.; Zaharieva, I.; Baktash, E.; Pfrommer, J.; Schwarze, M.; Dau, H.; Driess, M. *Angew. Chem. Int. Ed.* **2013**, *52*, 13206-13210.

(8) Shevela, D.; Koroidov, S.; Najafpour, M. M.; Messinger, J.; Kurz, P. *Chem. Eur. J.* **2011**, *17*, 5415-5423.

(9) Robinson, D. M.; Go, Y. B.; Mui, M.; Gardner, G.; Zhang, Z.; Mastrogiovanni, D.; Garfunkel, E.; Li, J.; Greenblatt, M.; Dismukes, G. C. *J. Am Chem. Soc.* **2013**, *135*, 3494-3501.

(10) Gerken, J. B.; McAlpin, J. G.; Chen, J. Y. C.; Rigsby, M. L.; Casey, W. H.; Britt, R. D.; Stahl, S. S. *J. Am Chem. Soc.* **2011**, *133*, 14431-14442.

(11) Kent, C. A.; Concepcion, J. J.; Dares, C. J.; Torelli, D. A.; Rieth, A. J.; Miller, A. S.; Hoertz, P. G.; Meyer, T. J. *J. Am Chem. Soc.* **2013**, *135*, 8432-8435.

(12) Li, X. C.; Siegbahn, P. E. M. *J. Am Chem. Soc.* **2013**, *135*, 13804-13813.

(13) Vickers, J. W.; Lv, H. J.; Sumliner, J. M.; Zhu, G. B.; Luo, Z.; Musaev, D. G.; Geletii, Y. V.; Hill, C. L. *J. Am Chem. Soc.* **2013**, *135*, 14110-14118.

(14) McAlpin, J. G.; Stich, T. A.; Ohlin, C. A.; Surendranath, Y.; Nocera, D. G.; Casey, W. H.; Britt, R. D. *J. Am Chem. Soc.* **2011**, *133*, 15444-15452.

(15) Sun, K.; Saadi, F. H.; Lichterman, M. F.; Hale, W. G.; Wang, H. P.; Zhou, X. H.; Plymale, N. T.; Omelchenko, S. T.; He, J. H.; Papadantonakis, K. M.; Brunschwig, B. S.; Lewis, N. S. *Proc. Natl. Acad. Sci. USA* **2015**, *112*, 3612-3617.

(16) Morales-Guio, C. G.; Mayer, M. T.; Yella, A.; Tiley, S. D.; Gratzel, M.; Hu, X. L. *J. Am Chem. Soc.* **2015**, *137*, 9927-9936.

(17) Han, X. B.; Li, Y. G.; Zhang, Z. M.; Tan, H. Q.; Lu, Y.; Wang, E. B. *J. Am Chem. Soc.* **2015**, *137*, 5486-5493.

(18) Zou, X.; Goswami, A.; Asefa, T. *J. Am Chem. Soc.* **2013**, *135*, 17242-17245.

(19) Hong, D. C.; Yamada, Y.; Nagatomi, T.; Takai, Y.; Fukuzumi, S. *J. Am Chem. Soc.* **2012**, *134*, 19572-19575.

(20) Shao, M.; Zhang, R.; Li, Z.; Wei, M.; Evans, D. G.; Duan, X. *Chem. Commun.* **2015**, *51*, 15880-15893.

(21) Nguyen, A. I.; Ziegler, M. S.; Oña-Burgos, P.; Sturzbecher-Hohne, M.; Kim, W.; Bellone, D. E.; Tilley, T. D. *J. Am Chem. Soc.* **2015**, *137*, 12865-12872.

(22) Barnett, S. M.; Goldberg, K. I.; Mayer, J. M. *Nat. Chem.* **2012**, *4*, 498-502.

(23) Zhang, T.; Wang, C.; Liu, S.; Wang, J.-L.; Lin, W. *J. Am Chem. Soc.* **2014**, *136*, 273-281.

(24) Limburg, J.; Vrettos, J. S.; Liable-Sands, L. M.; Rheingold, A. L.; Crabtree, R. H.; Brudvig, G. W. *Science* **1999**, *283*, 1524-1527.

(25) Fillol, J. L.; Codolà, Z.; Garcia-Bosch, I.; Gómez, L.; Pla, J. J.; Costas, M. *Nat. Chem.* **2011**, *3*, 807-813.

(26) Park, J.; Kim, H.; Jin, K.; Lee, B. J.; Park, Y.-S.; Kim, H.; Park, I.; Yang, K. D.; Jeong, H.-Y.; Kim, J.; Hong, K. T.; Jang, H. W.; Kang, K.; Nam, K. T. *J. Am Chem. Soc.* **2014**, *136*, 4201-4211.

(27) Gonzalez-Flores, D.; Sanchez, I.; Zaharieva, I.; Klingan, K.; Heidkamp, J.; Chernev, P.; Menezes, P. W.; Driess, M.; Dau, H.; Montero, M. L. *Angew. Chem. Int. Ed.* **2015**, *54*, 2472-2476.

(28) Kanan, M. W.; Nocera, D. G. *Science* **2008**, *321*, 1072-1075.

(29) Liang, L.; Cheng, H.; Lei, F.; Han, J.; Gao, S.; Wang, C.; Sun, Y.; Qamar, S.; Wei, S.; Xie, Y. *Angew. Chem. Int. Ed.* **2015**, *54*, 12004-12008.

(30) Liu, Y.; Cheng, H.; Lyu, M.; Fan, S.; Liu, Q.; Zhang, W.; Zhi, Y.; Wang, C.; Xiao, C.; Wei, S.; Ye, B.; Xie, Y. *J. Am Chem. Soc.* **2014**, *136*, 15670-15675.

(31) Gao, M.-R.; Xu, Y.-F.; Jiang, J.; Zheng, Y.-R.; Yu, S.-H. *J. Am Chem. Soc.* **2012**, *134*, 2930-2933.

(32) Feng, L.-L.; Yu, G.; Wu, Y.; Li, G.-D.; Li, H.; Sun, Y.; Asefa, T.; Chen, W.; Zou, X. *J. Am Chem. Soc.* **2015**, *137*, 14023-14026.

(33) Patil, S. A.; Kim, E.-K.; Shrestha, N. K.; Chang, J.; Lee, J. K.; Han, S.-H. *ACS Appl. Mat. Interfaces* **2015**, *7*, 25914-25922.

(34) Wang, K.; Ye, Z.; Liu, C.; Xi, D.; Zhou, C.; Shi, Z.; Xia, H.; Liu, G.; Qiao, G. *ACS Appl. Mat. Interfaces* **2016**, *8*, 2910-2916.

(35) Tengner, S. *Z. Anorg. Allg. Chem.* **1938**, *239*, 126-132.

(36) Li, H. H.; Zhang, P.; Liang, C. L.; Yang, J.; Zhou, M.; Lu, X. H.; Hope, G. A. *Cryst. Res. Technol.* **2012**, *47*, 1069-1074.

(37) Biesinger, M. C.; Payne, B. P.; Grosvenor, A. P.; Lau, L. W. M.; Gerson, A. R.; Smart, R. S. C. *Appl. Surf. Sci.* **2011**, *257*, 2717-2730.

(38) Dupin, J. C.; Gonbeau, D.; Benqlilou-Moudden, H.; Vinatier, P.; Levasseur, A. *Thin Solid Films* **2001**, *384*, 23-32.

(39) Wang, Z.; Wang, W.; Yang, Y.; Li, W.; Feng, L.; Zhang, J.; Wu, L.; Zeng, G. *Int. J. Photoenergy* **2014**, *2014*, 6.

(40) Nohira, H.; Tsai, W.; Besling, W.; Young, E.; Petry, J.; Conard, T.; Vandervorst, W.; De Gendt, S.; Heyns, M.; Maes, J.; Tuominen, M. *J. Non-Cryst. Solids* **2002**, *303*, 83-87.

(41) Jeon, H. S.; Jee, M. S.; Kim, H.; Ahn, S. J.; Hwang, Y. J.; Min, B. K. *ACS Appl. Mat. Interfaces* **2015**, *7*, 24550-24555.

(42) McCrory, C. C. L.; Jung, S.; Peters, J. C.; Jaramillo, T. F. *J. Am Chem. Soc.* **2013**, *135*, 16977-16987.

(43) Gao, M.; Sheng, W.; Zhuang, Z.; Fang, Q.; Gu, S.; Jiang, J.; Yan, Y. *J. Am Chem. Soc.* **2014**, *136*, 7077-7084.

(44) Blöchl, P. E. *Phys. Rev. B* **1994**, *50*, 17953-17979.

(45) Kresse, G.; Hafner, J. *Phys. Rev. B* **1994**, *49*, 14251-14269.

(46) Kresse, G.; Furthmüller, J. *Phys. Rev. B* **1996**, *54*, 11169-11186.

(47) Kresse, G.; Joubert, D. *Phys. Rev. B* **1999**, *59*, 1758-1775.

(48) Peng, H.; Yang, Z.-H.; Sun, J.; Perdew, J. P. *arXiv:1510.05712, Phys. Rev.* **2015**, to appear.

(49) Sun, J.; Ruzsinszky, A.; Perdew, J. P. *Phys. Rev. Lett.* **2015**, *115*, 036402.

(50) Vydrov, O. A.; Van Voorhis, T. *J. Chem. Phys.* **2010**, *133*, 244103-244106.

(51) Sabatini, R.; Gorni, T.; de Gironcoli, S. *Phys. Rev. B* **2013**, *87*, 041108.

(52) Perdew, J. P.; Burke, K.; Ernzerhof, M. *Phys. Rev. Lett.* **1996**, *77*, 3865-3868.

(53) Cady, C. W.; Gardner, G.; Maron, Z. O.; Retuerto, M.; Go, Y. B.; Segan, S.; Greenblatt, M.; Dismukes, G. C. *ACS Catal.* **2015**, *5*, 3403-3410.

(54) Suntivich, J.; May, K. J.; Gasteiger, H. A.; Goodenough, J. B.; Shao-Horn, Y. *Science* **2011**, *334*, 1383-1385.

(55) Monkhorst, H. J.; Pack, J. D. *Phys. Rev. B* **1976**, *13*, 5188-5192.

(56) Tae, E. L.; Song, J.; Lee, A. R.; Kim, C. H.; Yoon, S.; Hwang, I. C.; Kim, M. G.; Yoon, K. B. *ACS Catal.* **2015**, *5*, 5525-5529.